MATERIALS CHEMISTRY
FRONTIERS

RESEARCH ARTICLE

View Article Online
View Journal | View Issue

Check for updates

Cite this: *Mater. Chem. Front.*, 2018, **2**, 2109

Gamma radiation-responsive side-chain tellurium-containing polymer for cancer therapy†

Fuqiang Fan,‡[ab] Shiqian Gao,‡[bc] Shaobo Ji,[b] Yu Fu,*[a] Pengpeng Zhang*[d] and Huaping Xu *[b]

Received 2nd July 2018,
Accepted 13th September 2018

DOI: 10.1039/c8qm00321a

rsc.li/frontiers-materials

The combination of chemotherapy and radiotherapy could not only enhance cancer treatment efficacy, but also shorten the period of the overall treatment and relieve the anxiety of the patients during the remedy. Herein, we present a novel strategy for coordinating the chemotherapy drug CDDP with a tellurium-containing polymer, which restrained the tumour cytotoxicity of these two portions. After a low dose of γ radiation, CDDP departed from the coordination complexes, and the tumour cytotoxicity of both was restored. In contrast to conventional chemotherapy, this radiation responsive system possesses specific anticancer effects and less toxicity in the non-radiation therapy. In addition, with regard to the premise of therapeutic efficiency, this system effectively lowered the radiated dosage.

Published on 14 September 2018. Downloaded on 2/22/2026 8:50:49 PM.

Introduction

Due to its high incidence rate and death rate, cancer is a serious threat to human health and lives.[1] Recently, diverse treatments have been developed,[2,3] including surgical treatments, chemotherapy,[4–6] radiotherapy,[7,8] immunotherapy,[9–11] and photodynamic therapy.[12–14] Among these, chemotherapy and radiotherapy are two of the most conventional and effective treatment methods.

Nevertheless, besides their own advantages, both chemotherapy and radiotherapy have inevitable shortcomings and deficiencies. Chemotherapeutics, such as cisplatin (CDDP), oxaliplatin, and carboplatin, are all effective cancer medicaments. CDDP has been widely used in clinics since its authorization by the US Food and Drug Administration (FDA) in 1987.[15–17] However, the application of CDDP is limited by its severe side effects, short circulation period and easy deactivation. Radiotherapy is also a powerful tool for cancer treatment with the advantage of its ability to be adjusted over time and locations. However, radiotherapy is impeded due to its health hazards, irradiation dose, irradiation resistance, *etc.*[8] Nanomedicine is an effective method to prolong the drug half-time and reduce the side effects. Numerous stimuli-responsive characteristics also endow nanomedicine with more function in precise cancer therapy.[18–22] Among them, gamma radial, as an exogenous stimulus, could be used to trigger drug release.

Tellurium and selenium are located in the same group within the periodic table of elements. The antitumor activity of selenium is attributed to its function of regulating the reactive oxygen species concentration *in vivo*.[23–30] Compared with selenium, tellurium is not an essential biological trace element. However, tellurium is also a bioactive element and shows a range of unique properties,[31,32] such as antioxidant activity,[33–35] activity against pathogenic microorganisms,[36,37] and inhibition of the growth of cancer cells.[38–44] The chemistry of tellurium is rich in inorganic substances, including tellurium quantum dots, various salts and a wide range of diverse organotellurium compounds. The toxic effects of tellurium depend on its chemical form. Many studies have revealed that the toxic effects of tellurium are due to redox modulation.[45,46] Tellurium-containing compounds have the ability to generate ROS, increase oxidative stress, and convert less-reactive ROS into a high-reactive species. Our research group previously designed and synthesized a series of tellurium-containing polymers for drug delivery and stimuli-responsive materials.[47–51] Tellurium benefits include its coordination effect and its ultra-sensitive redox reaction, and a tellurium-containing polymer provides an opportunity for combining chemotherapy and radiotherapy. A lower dosage is the precondition for radiotherapy. The benefit of high sensitivity of tellurium to ROS makes tellurium-containing polymers suitable for radiotherapy. An ideal drug for cancer treatment should be selectively switched on in the tumorous microenvironment by responding to the external stimulus while staying inert during its systemic circulation. Herein, we synthesized a side-chain tellurium-containing

[a] *College of Sciences, Northeastern University, Shenyang 110819, China. E-mail: fuyu@mail.neu.edu.cn*
[b] *Key Lab of Organic Optoelectronics & Molecular Engineering, Department of Chemistry, Tsinghua University, Beijing 100084, China. E-mail: xuhuaping@mail.tsinghua.edu.cn*
[c] *Tsinghua-Peking Joint Center for Life Sciences, Beijing 100084, China*
[d] *Department of Respiratory and Critical Care Medicine, Jinling Hospital, 305 East Zhongshan Road, Nanjing 210002, China. E-mail: pp_nz@163.com*
† Electronic supplementary information (ESI) available. See DOI: 10.1039/c8qm00321a
‡ These authors contributed equally.

Published on 14 September 2018. Downloaded on 2/22/2026 8:50:49 PM.

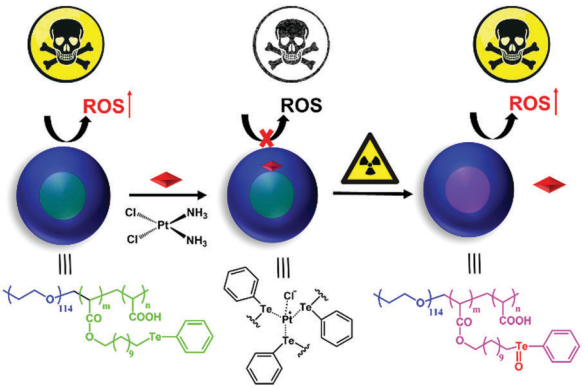

Scheme 1 The gamma stimuli-responsive tellurium-containing coordination complexes.

amphiphilic polymer, PEG-*b*-PAA-*g*-Te. The polymer coordinated with CDDP and self-assembled in an aqueous solution with CDDP in the hydrophobic core of the nanoparticles. Due to the coordination effect, the cytotoxicity of the coordination complexes is sheltered temporarily, which decreases the side effects of the nanomedicine. After a low dosage of γ radiation, the tellurium-containing block of the nanoparticles is oxidized. The oxidized group (Te═O) improves the hydrophilicity of the entire block of nanoparticles and hence, the nanoparticles tend to disassemble. Oxidization weakens the coordination between CDDP and Te, due to which CDDP departs from the nanoparticles, leading to recovery of the tumour cytotoxicity of the complexes. Additional results proved that the tellurium in the nanoparticles elevated the concentration of reactive oxygen species (ROS) in cells, which induced cell apoptosis. After coordinating with CDDP, the ROS-induced ability of tellurium decreased significantly. Interestingly, a low dosage radiation recovered the ROS-regulation ability of tellurium and caused further cell death. A strategy for combining chemotherapy and radiotherapy in one system is proposed in this study. The system endows chemotherapy with a target, reduces the dosage of radiation, and achieves the goal of complementary advantages of the synergistic treatment (Scheme 1).

Results and discussion

Synthesis of the tellurium-containing polymer (PEG-*b*-PAA-*g*-Te)

Through an acyl chloride–ol esterification, the side-chain tellurium-containing polymer was synthesized. Since PEG-*b*-PAA is a double hydrophilic block copolymer, it does not self-assemble in an aqueous environment. By grafting the carboxyl group of PAA with hydrophobic alkyl tellurium molecule Ar–Te–OH, we obtained an amphiphilic tellurium-containing block polymer (PEG-*b*-PAA-*g*-Te). The synthesis routes are shown in Fig. 1. According to the feed ratio, we synthesized two grafting ratios, PEG-*b*-PAA-*g*-Te-40 and PEG-*b*-PAA-*g*-Te-100. The ^{1}H NMR measurement confirmed the successful synthesis of Ar–Te–OH (Fig. S1, ESI†) and PEG-*b*-PAA-*g*-Te (Fig. S2, ESI†). The grafting ratio was calculated from the ^{1}H NMR spectra by comparing the peak area of the ethylene oxide protons at 3.64 ppm with the α-protons of tellurium at

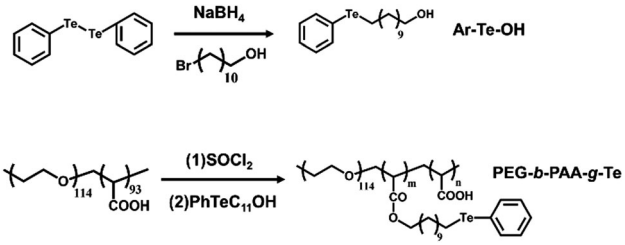

Fig. 1 Synthesis route of PEG-*b*-PAA-*g*-Te.

2.90 ppm. We synthesized two grafting ratio polymers with ratio of 40% (Te-40) and 100% (Te-100). The 100% grafting ratio polymers were chosen for the subsequent study.

Coordination of Ar–Te–OH with CDDP

First, we studied the coordination behaviour between platinum and tellurium. Distinct from our previous research on the alkyl chain of tellurium molecules, the tellurium-containing aromatic molecules had different abilities to coordinate with platinum-based anticancer drugs. Herein, we chose CDDP to coordinate with Ar–Te–OH. The coordination interaction was confirmed by ^{1}H NMR and XPS. The deshielding effect of Pt^{2+} resulted in the shift of the α-proton of tellurium from 2.90 ppm to 3.15 ppm (Fig. S3, ESI†). Furthermore, the XPS results provided more evidences. After coordination, the 3d peaks of tellurium shifted from 572.02 eV and 582.35 eV to 574.52 eV and 585.02 eV, respectively (Fig. 2a). The ESI-mass spectrum provided more details about the coordination complexes. The highest peak was found at 1359.29 (Fig. 2b), which was ascribed to the molecular formula of $[Pt(PhTeC_{11}OH)_3Cl]^+$, which indicated the maximum coordination ratio of 3 : 1.

Assembly and gamma response of the PEG-*b*-PAA-*g*-Te based nanoparticles

PEG-*b*-PAA-*g*-Te was an amphiphilic block polymer that self-assembled in water. The diameter of the nanoparticles was approximately 33 nm, which was obtained by the dynamic light scattering (DLS) measurement (Fig. S5a, ESI†). The transmission electron microscopy (TEM) analysis of the nanoparticles confirmed

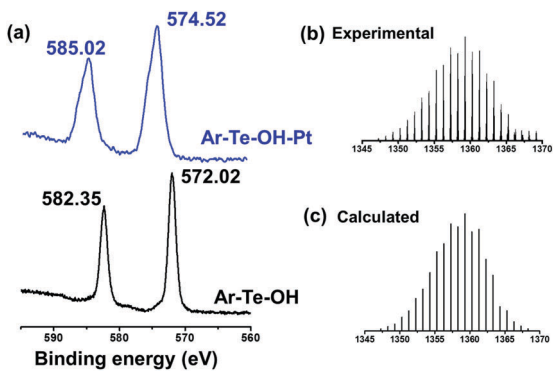

Fig. 2 The coordination interaction of Ar–Te–OH with CDDP. (a) The XPS spectra of the Te^{3d} before and after coordination with CDDP. Experimental (b) and calculated (c) ESI-MS signals for the coordination complexes.

 This journal is © The Royal Society of Chemistry and the Chinese Chemical Society 2018

Published on 14 September 2018. Downloaded on 2/22/2026 8:50:49 PM.

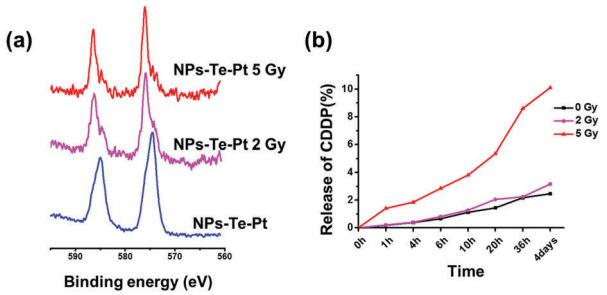

Fig. 3 (a) The XPS spectra of Te 3d in the nanoparticles after γ radiation. (b) CDDP release profiles after gamma radiation measured by ICP-MS.

a size, which was consistent with the DLS result, and the spherical morphology (Fig. S5b, ESI†). After coordinating with CDDP, the morphology of the nanoparticles did not change, except for a slight decrease in diameter (Fig. S5a and S5c, ESI†). The diameter decrease could be attributed to the multi-dentate ligand between tellurium and platinum, which played a part in crosslinking. Due to the coordination interaction between tellurium and platinum, CDDP was mainly packaged within the hydrophobic layer of the nanoparticles, which guaranteed the drug's high stability and avoided the leaking problem. The encapsulation efficiency and loading content of CDDP were 35.8% and 6.7%, respectively. Under a low dosage γ radiation, the nanoparticles tend to disassemble, and the trend is clearer on increasing the radiation dosage (Fig. S6, ESI†). The XPS spectrum confirmed the oxidation of tellurium in the nanoparticles after radiation (Fig. 3a), resulting in the release of CDDP from the nanoparticles. According to our previous study,[25] γ radiation induced the generation of ROS, and the ROS oxidized the tellurium block in the nanoparticles. After the radiation, the coordination bond was broken, but CDDP was still in the hydrophobic layer of the nanoparticles. Due to the oxidized group (Te═O), the entire block of nanoparticles showed an improved hydrophilicity. CDDP departed from the hydrophobic layer and was continuously released from the nanoparticles. The 2 Gy radiation was a relatively low dosage and induced partial oxidation of the tellurium. Most of the CDDP was still in the nanoparticles. However, 5 Gy radiation was enough to oxidize most of the tellurium in the nanoparticles, and CDDP was gradually released. This drug-release system did not show an obvious burst release (Fig. 3b).

Cellar uptake and distribution

A high uptake level is a precondition for efficient drug delivery. We encapsulated Dox as a fluorescence indicator in the nanoparticles to investigate the cellar uptake and distribution of the nanoparticles. MDA-MB-231 cells were incubated with PEG-*b*-PAA-*g*-Te/Dox and were examined at various times with a flow cytometer. The cellular fluorescence intensity increased over time, suggesting that the nanoparticles were internalized continuously (Fig. S7a and b, ESI†). The confocal microscopy results showed an intracellular distribution of the nanoparticles. After 4 h of incubation with the MDA-MB-231 cell, most of the nanoparticles were found to be located in the cytoplasm

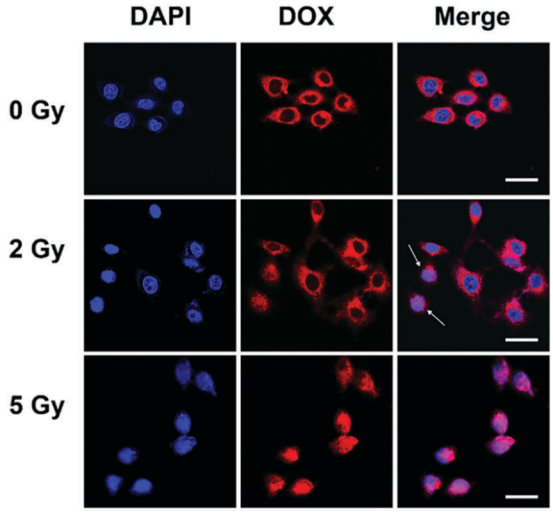

Fig. 4 Cellular uptake and distribution of the nanoparticles. Confocal microscopic images of the intracellular distribution of PEG-*b*-PAA-*g*-Te/Dox. The scale bar is 25 μm.

after endocytosis. The encapsulated Dox was stable unless there were radical stimuli. With a low dosage radiation, the encapsulated Dox released and entered into the cell nucleus (Fig. 4). The released Dox was located at the same organelle as the free Dox (Fig. S8, ESI†). This result was another proof for the disassembly of the nanoparticles under gamma radiation in the cellular environment.

In vitro cytotoxicity study

Next, we detected the cancer cell killing effect of this gamma radiation responsive nanomedicine by using CCK-8 assay. PEG-*b*-PAA was a biocompatible water-soluble polymer, which had no cytotoxicity to MDA-MB-231 cells (Fig. S9a, ESI†). After grafting the tellurium-containing molecules, PEG-*b*-PAA-*g*-Te showed an evident killing activity towards the A549, HepG2, and MDA-MB-231 cell lines. As shown in Fig. S9b (ESI†), the killing activity of the nanoparticles depended on the grafting ratio of tellurium. The 100% grafting polymer (Te-100) showed a more significant killing activity than the 40% (Te-40). Importantly, after coordination with CDDP, the killing activity of the coordination complexes was sheltered temporarily. Coordination with platinum dichloride also showed the same results (Fig. 5a and Fig. S10, ESI†). The coordination bond was broken by γ radiation, and the killing activity of the nanoparticles was recovered. After γ radiation, the coordination complexes were co-incubated with MDA-MB-231 or HepG2 cells for 48 h. As shown in Fig. 5b, a low dosage radiation decreased the coordination ability between tellurium and platinum. CDDP departed from the nanoparticles, and the killing activity of both was recovered to some extent.

To investigate the effect of the synergistic treatment of chemotherapy and radiotherapy, 100 μg mL^{-1} of the PEG-*b*-PAA-*g*-Te/CDDP coordinated complexes was added to the MDA-MB-231 cells along with radiation treatment. Then, 72 h later, the cell viability was quantified. The cytotoxicity of the

Published on 14 September 2018. Downloaded on 2/22/2026 8:50:49 PM.

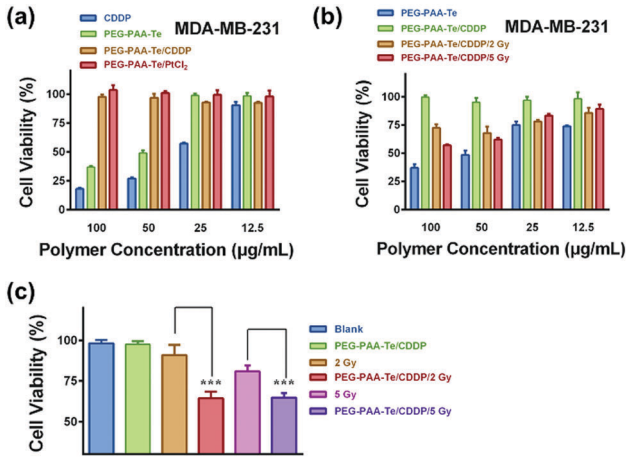

Fig. 5 Cytotoxicity of the different nanoparticles *in vitro*. (a) PEG-*b*-PAA-*g*-Te and the different coordination complexes. (b) PEG-*b*-PAA-*g*-Te, the coordination complexes and the coordination complexes after radiation. (c) Radiation with and without the coordination complexes. ***$p < 0.001$.

irradiated PEG-*b*-PAA-*g*-Te/CDDP group was significantly higher than that of other groups (Fig. 5c). The flow cytometry analysis confirmed the advantage of the synergistic treatment in cancer cell apoptosis (Fig. 6). The blank/2 Gy (4.76%) or Blank/5 Gy group (10.44%) did not have distinct treatment effect because of the low dosage of radiation. The CDDP alone group increased the cell apoptosis portion (17.47%), and the irradiation could further enhance it. However, this synergetic chemotherapy was non-targeting and could not avoid the side effect of CDDP (Fig. S11, ESI†). The PEG-*b*-PAA-*g*-Te/CDDP synergistic group was inert without stimuli (0.27%). Interestingly, the killing activity of the coordination complexes switched on under γ radiation, while PEG-*b*-PAA-*g*-Te/CDDP/2 Gy and PEG-*b*-PAA-*g*-Te/CDDP/5 Gy induced 17.23% and 15.31% cell apoptosis, respectively (Fig. 6). In this way, we achieved the purpose of the complementary advantages of the synergistic treatment. The synergistic treatment showed a high gamma responsiveness and controllable killing activity, which guaranteed the effect of the treatment. Radiation

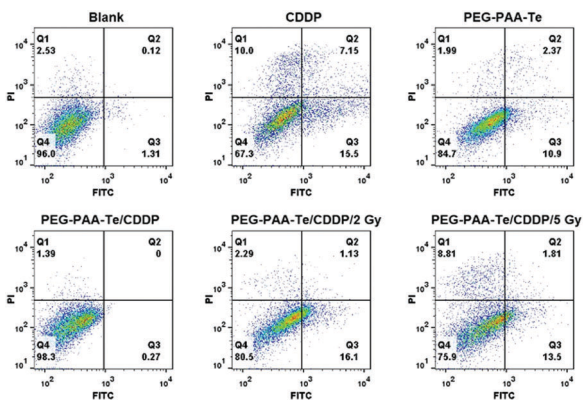

Fig. 6 Flow cytometry measured the cell apoptosis of the different nanoparticles. The sum of the *Q2* and *Q3* areas indicated the cell apoptosis.

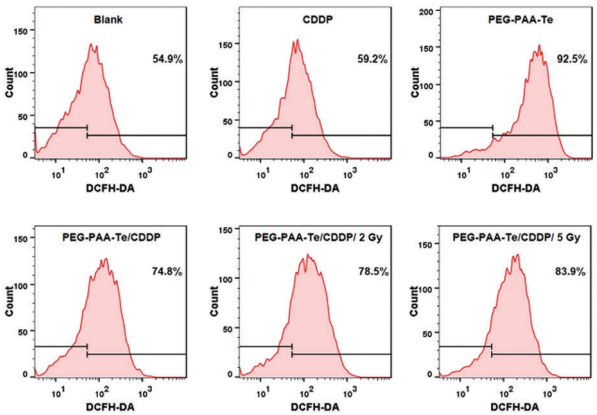

Fig. 7 Flow cytometry images. The concentration of the reactive oxygen species treated with the different nanoparticles.

triggered the function of the chemotherapy, while chemotherapy reduced the treatment dosage of the radiotherapy.

Mechanism of the cytotoxicity

Selenium could regulate the concentration of the reactive oxygen species (ROS) *in vivo* and further induce cell apoptosis. To investigate whether the tellurium-containing nanoparticles possessed a similar ability, a reactive oxygen kit was used to monitor the concentration of ROS in the cell. After a 30 min incubation with the ROS assay kit, the fluorescence signals (Fig. 7) and the caspase-3 activity of the cells were measured (Fig. S12b, ESI†). According to the results, PEG-*b*-PAA-*g*-Te elevated the concentration of ROS in the cell. When tellurium was coordinated with platinum, the ROS-induced ability of PEG-*b*-PAA-*g*-Te/CDDP was restrained. With γ radiation (PEG-*b*-PAA-*g*-Te/CDDP/2 Gy and PEG-*b*-PAA-*g*-Te/CDDP/5 Gy), the inhibiting effect was removed, and the ROS-induced ability of tellurium was recovered. Caspases are cysteine proteases that play an important role in cell apoptosis. Caspase-3 acts as a central regulator of cell apoptosis. To investigate the signalling pathways of the PEG-*b*-PAA-*g*-Te nanoparticles, a fluorometric assay was applied to monitor the activation of caspase-3 in the cell. As shown in Fig. S12b (ESI†), PEG-*b*-PAA-*g*-Te NPs caused the activation of caspase-3. After coordinating with CDDP (PEG-PAA-Te/Pt), the induced ability was restrained. With 5 Gy irradiation, the activation of caspase-3 significantly increased. These results showed that the cancer killing mechanism of the tellurium-containing nanoparticles would be related to the ROS regulation and caspase-3 apoptosis pathway activation.

Conclusion

In summary, by a coordination effect with CDDP and the γ responsiveness of tellurium, chemotherapy and radiotherapy were integrated into one nanomedicine system. The tellurium-containing coordination complexes remained inert during the prolonged circulation, and the killing activity was triggered by γ radiation at the tumorous sites. This system may open a new avenue for the further development of synergistic therapies.

 This journal is © The Royal Society of Chemistry and the Chinese Chemical Society 2018

Published on 14 September 2018. Downloaded on 2/22/2026 8:50:49 PM.

Experimental

Materials and methods

Materials and reagents. Sodium borohydride and thionyl chloride were purchased from the Aladdin chemical company. 11-Bromoundecanol, CDDP, trimethylamine, diphenyl ditelluride, and superdry *N,N*-dimethylformamide (DMF) were purchased from J&K Scientific Ltd. Poly(ethyleneoxide-*b*-acrylic acid) (PEG_{144}–PAA_{93}, PDI = 1.2, M_n = 5000-*b*-6700) was purchased from Polymer Source. Other organic solvents were procured from the Beijing Chemical Reagent Company.

Characterizations

The ^{1}H NMR spectra were recorded on a JEOL-ECA 400 (400 MHz). The size distribution of the nanoparticles was measured by a Zetasizer nano ZS90 (Malvern Instruments, Malvern, UK), using a monochromatic coherent He–Ne laser (633 nm). Transmission electron microscopy (TEM) images were obtained on a JEM-2010 microscope, and the samples were stained with a 2% uranyl acetate solution. The X-ray photoelectron spectroscopy (XPS) was performed using a PHI Quantera scanning X-ray microprobe. The electrospray ionization mass spectrometry (ESI-MS) was conducted on an LTQ LC/MS apparatus. The inductively coupled plasma mass spectrometry measurement was obtained on an ELAN DRC-e ICP Mass Spectrometer. Flow cytometry was performed using a BD Calibur and BD FACSAria III.

Synthesis of Ar–Te–OH

A total of 0.8 g (1.95 mmol) of diphenyl ditelluride and 0.1 g (2.64 mmol) of sodium borohydride were added to 10 mL of water and 30 mL of THF in a 200 mL flask at 50 °C. The flask was gently shaken, and sealed using a rubber plug (caution gas generated). When the solution turned colourless, 0.98 g (3.90 mmol) of 11-bromoundecanol in 20 mL of THF was injected into the mixture. The reaction was stirred at 50 °C overnight. After cooling to room temperature, the mixture was extracted with saturated brine and DCM. The organic layer was washed using saturated brine twice and was dried and evaporated. Then, a white solid was obtained. The raw product was further purified by column chromatography with DCM as the eluent. Finally, white power (1.2 g) was obtained (70% yield). ^{1}H NMR (400 MHz, $CDCl_3$) δ (ppm): 7.00–8.00 (5H, C_6H_5), 3.63 (2H, CH_2OH), 2.90 (2H, $TeCH_2$), and 2.00–1.25 (18H, $TeCH_2(CH_2)_9CH_2OH$).

Synthesis of PEG-*b*-PAA-*g*-Te

A total of 0.10 g of PEG-*b*-PAA (−COOH 0.80 mmol) was dissolved in 8 mL of $SOCl_2$, and the solution was refluxed overnight. The solvent was removed by distillation under vacuum, and 0.5 g of Ar–Te–OH in 10 mL of anhydrous DMF was added to the flask with 1.0 mL of trimethylamine. The reaction mixture was stirred at 50 °C overnight. After the evaporation of DMF, the solid was added to a sodium borohydride aqueous solution to obtain a micellar solution, and the pH was adjusted to acidic. The solution was extracted using saturated brine and DCM. After drying and evaporating the organic layer, a dark brown solid was obtained. The grafting ratio was calculated using ^{1}H-NMR spectroscopy by comparing the peak area of the ethylene oxide protons at 3.64 ppm with the α-protons of tellurium at 2.90 ppm. ^{1}H NMR (400 MHz, DMSO-D_6) δ (ppm): 7.00–8.00 (5H, C_6H_5), 4.04 (2H, $COOCH_2$), 3.63 (4H, OCH_2CH_2 of PEG), 2.90 (2H, $TeCH_2$), and 2.00–1.25 (18H, $TeCH_2(CH_2)_9CH_2O$).

Coordination of PEG-*b*-PAA-*g*-Te with CDDP

PEG-*b*-PAA-*g*-Te and cisplatin were dissolved in DMSO and kept in a shaker at 37 °C before further characterization. The encapsulation efficiency and loading content were calculated by the following equations. Encapsulation efficiency = $(A - B)/A \times 100\%$, where A was the initial amount of drug added in the system and B was the amount remaining in the system. Loading content = $(A - B)/C \times 100\%$, where A represented the initial amount of the drug, B represented remaining amount of the drug and C represented the amount of PEG-*b*-PAA-*g*-Te polymer.

Assembly of nanoparticles

A total of 10.0 mg PEG-*b*-PAA-*g*-Te and 5.0 mg CDDP were dissolved in 1 mL DMSO to coordinate for 7 days. Then, the solution was slowly added into 10 mL deionized water under sonication. Following this, the solvent was dialysed against with deionized water for more than 24 h. The solution was diluted to 20 mL to obtain a concentration of 0.5 mg mL^{-1} for the further experiments.

CDDP release profiles

The amount of CDDP released was determined by inductively coupled plasma spectrometry. The release rate was calculated by the following equation: $B/A \times 100\%$, where A was the initial amount of drug encapsulated in the system and B represented the amount of drug obtained in the solution.

Cell culture

Human lung carcinoma A549 cells, human liver carcinoma HepG2 cells and human breast carcinoma MDA-MB-231 cells were culture d in Dulbecco' s Modified Eagle Medium (DMEM) that was supplemented with 10% foetal bovine serum at 37 °C in a 5% CO_2 humidified atmosphere.

Cytotoxicity assay

The A549, HepG2, and MDA-MB-231 cells were seeded into 96-well plates at a density of 10 000 cells per well. After incubating the cell for 12 h, different drugs were added at different concentrations, and the cell viability was quantified by using a CCK-8 assay.

Imaging of the cells *in vitro*

Dox, as the fluorescence indictor, was encapsulated in the nanoparticles. The MDA-MB-231 cells were seeded onto a borosilicate chambered cover slides for 12 h. The PEG-*b*-PAA-*g*-Te/Dox nanoparticles were added and incubated at 37 °C for 4 h and then, the cells were washed three times with PBS and imaged with an LSM710 confocal microscope.

Published on 14 September 2018. Downloaded on 2/22/2026 8:50:49 PM.

Flow cytometry analysis

The MDA-MB-231 cells were seeded into 6-well plates at a density of 10 000 cells per well and 12 h later, various coordination complexes were added and co-incubated. The cells were washed three times with PBS and analyzed.

Statistical analysis

SPSS software was used for statistical analysis.

Conflicts of interest

The authors declare no competing financial interest.

Acknowledgements

This study was financially supported by the National Natural Science Foundation of China (Grant 21734006, 91427301), the National Basic Research Plan of China (2018YFA0208900), the National Science Foundation for Distinguished Young Scholars (Grant 21425416), and the Open Project of State Key Laboratory of Supramolecular Structure and Materials (sklssm201804, sklssm201822).

Notes and references

1 R. L. Siegel, K. D. Miller and A. Jemal, *Ca-Cancer J. Clin.*, 2017, **67**, 7–30.
2 Y. L. Wang, S. Y. Sun, Z. Y. Zhang and D. L. Shi, *Adv. Mater.*, 2018, **30**, 1705660.
3 S. L. Kim, S. J. Choi, H. J. Cho and I. D. Kim, *Acc. Chem. Res.*, 2017, **50**, 1587–1596.
4 K. Zhang, Z. Yang, X. D. Meng, Y. Cao, Y. D. Zhang, W. H. Dai, H. T. Lu, Z. F. Dong and X. J. Zhang, *Mater. Chem. Front.*, 2018, **2**, 1184–1195.
5 Y. Zhao and M. D. Pluth, *Angew. Chem., Int. Ed.*, 2016, **55**, 14638–14642.
6 Z. Z. Yue, H. Wang, Y. M. Li, Y. Qin, L. Xu, D. J. Bowers, M. Gangoda, X. P. Li, H. B. Yang and Y. R. Zheng, *Chem. Commun.*, 2018, **54**, 731–734.
7 H. Huang, L. Z. He, W. H. Zhou, G. B. Qu, J. H. Wang, J. H. Yang, N. Yang, J. Gao, T. F. Chu, K. Paul and X. F. Yu, *Biomaterials*, 2018, **171**, 12–22.
8 R. Yahyapour, E. Motevaseli, A. Rezaeyan, H. Abdollahi, B. Farhood, M. Cheki, M. Najafi and V. Villa, *Curr. Radiopharm.*, 2018, **11**, 34–45.
9 D. M. Pardoll, *Nat. Rev. Cancer*, 2012, **12**, 252–264.
10 S. A. Rosenberg, J. C. Yang and N. P. Restifo, *Nat. Med.*, 2004, **10**, 909–915.
11 A. P. Castano, P. Mroz and M. R. Hamblin, *Nat. Rev. Cancer*, 2006, **6**, 535–545.
12 M. M. Lerch, M. J. Hansen, G. M. van Dam, W. Szymanski and B. L. Feringa, *Angew. Chem., Int. Ed.*, 2016, **55**, 10978–10999.
13 O. Babii, S. Afonin, L. V. Garmanchuk, V. V. NIkulina, T. V. Nikolaienko, O. V. Storozhuk, D. V. Shelest, O. I. Dasyukevich, L. I. Ostapchenko, V. Iurchenko, S. Zozulya, A. S. Ulrich and I. V. Komarov, *Angew. Chem., Int. Ed.*, 2016, **55**, 5493–5497.
14 Y. S. Chen, S. J. Yoon, W. Frey, M. Dockery and S. Emelianov, *Nat. Commun.*, 2017, **8**, 15782–16792.
15 W. P. McGuire, W. J. Hoskins, M. F. Brady, P. R. Kucera, E. E. Partridge, K. Y. Look, D. L. Clarkepearson and M. Davidson, *N. Engl. J. Med.*, 1996, **334**, 1–6.
16 M. A. Barry, C. A. Behnke and A. Eastman, *Biochem. Pharmacol.*, 1990, **40**, 2353–2362.
17 T. Helleday, E. Petermann, C. Lundin, B. Hodgson and R. A. Sharma, *Nat. Rev. Cancer*, 2008, **8**, 193–204.
18 C. B. He, D. M. Liu and W. B. Lin, *Chem. Rev.*, 2015, **115**, 11079–11108.
19 W. Cui, J. B. Li and G. Decher, *Adv. Mater.*, 2016, **28**, 1302–1311.
20 Q. Y. Hu, W. J. Sun, C. G. Qian, C. Wang, H. N. Bomba and Z. Gu, *Adv. Mater.*, 2015, **27**, 7043–7050.
21 S. J. Kim, S. J. Choi, J. S. Jang, H. J. Cho and I. D. Kim, *Acc. Chem. Res.*, 2017, **50**, 1587–1596.
22 A. Kumar, S. Kim and J. M. Nam, *J. Am. Chem. Soc.*, 2016, **138**, 14509–14525.
23 A. A. Forastiere, H. Goepfert, M. Maor, T. F. Pajak, R. Weber, W. Morrison, B. Glisson, A. Trotti, J. A. Ridge, C. Chao, G. Peters, D. J. Lee, A. Leaf, J. Ensley and J. Cooper, *N. Engl. J. Med.*, 2003, **349**, 2091–2098.
24 J. Brognard, A. S. Clark, Y. C. Ni and P. A. Dennis, *Cancer Res.*, 2001, **61**, 3986–3997.
25 W. Cao, Y. W. Gu, M. Meineck and H. P. Xu, *Chem. – Asian J.*, 2014, **9**, 48–57.
26 T. Y. Li, W. T. Xiang, Y. Yi, Y. L. Chen, L. Cheng, Z. Liu and H. P. Xu, *ACS Appl. Mater. Interfaces*, 2016, **8**, 22106–22112.
27 T. Y. Li, W. T. Xiang, F. Li and H. P. Xu, *Biomaterials*, 2018, **157**, 17–25.
28 H. P. Xu, W. Cao and X. Zhang, *Acc. Chem. Res.*, 2013, **46**, 1647–1658.
29 F. Li, T. Y. Li, C. X. Sun, J. H. Xia, Y. Jiao and H. P. Xu, *Angew. Chem., Int. Ed.*, 2017, **56**, 9910–9914.
30 J. T. Rotruck, A. L. Pope, H. E. Ganther, A. B. Swanson, D. G. Hafeman and W. G. Hoekstra, *Science*, 1973, **179**, 588–590.
31 S. T. Manjare, Y. Kim and D. G. Churchill, *Acc. Chem. Res.*, 2014, **47**, 2985–2998.
32 L. A. Ba, M. Doring, V. Jamier and C. Jacob, *Org. Biomol. Chem.*, 2010, **8**, 4203–4216.
33 J. Malmstrom, M. Jonsson, I. A. Cotgreave, L. Hammarstrom, M. Sjodin and L. Engman, *J. Am. Chem. Soc.*, 2001, **123**, 3434–3440.
34 S. Griffin, M. Sarfraz, S. F. Hartmann, S. R. Pinnapireddy, M. J. Nasim, U. Bakowsky, C. M. Keck and C. Jacob, *Antioxidants*, 2018, **7**, 23–42.
35 M. Mcnaughton, L. Engman, A. Birmingham, G. Powis and I. A. Cotgreave, *J. Med. Chem.*, 2004, **47**, 233–239.
36 Z. S. Lu, C. M. Li, H. F. Bao, Y. Qiao, Y. H. Toh and X. Yang, *Langmuir*, 2008, **24**, 5445–5452.
37 A. Totchieva, G. Sisson, L. J. Bryden, D. E. Taylor and P. S. Hoffman, *Microbiology*, 2003, **149**, 1285–1295.

 This journal is © The Royal Society of Chemistry and the Chinese Chemical Society 2018

38 A. Angeli, T. Damiano, C. Antonella and C. T. Supuran, *Bioorg. Chem.*, 2018, **76**, 268–272.
39 B. Sredni, R. R. Caspi, A. Klein, Y. Kalechman, Y. Danziger, M. BenYaakov, T. Tamari, F. Shalit and M. Albeck, *Nature*, 1987, **330**, 173–176.
40 C. W. Nogueira, G. Zeni and J. B. T. Rocha, *Chem. Rev.*, 2004, **104**, 6255–6286.
41 L. J. Edgar, R. N. Vellanki, A. Halupa, D. Hedley, B. G. Wouters and M. NItz, *Angew. Chem., Int. Ed.*, 2014, **53**, 11473–11477.
42 Y. Kalechman, U. Gafter, R. Gal, G. Rushkin, D. H. Yan, M. Albeck and B. Sredni, *J. Immunol.*, 2002, **169**, 384–392.
43 B. Sredni, M. Weil, G. Khomenok, I. Lebenthal, S. Teitz, Y. Mardor, Z. Ram, A. Orenstein, A. Kershenovich, S. Michowiz, Y. I. Cohen, Z. H. Rappaport, I. Freidkin, M. Albeck, D. L. Longo and Y. Kalechman, *Cancer Res.*, 2004, **64**, 1843–1852.
44 G. Halpert, T. Eitan, E. Voronov, R. N. Apte, L. Rath-Wolfson, M. Albeck, Y. Kalechman and B. Sredni, *J. Biol. Chem.*, 2014, **289**, 17215–17227.
45 L. A. Ba, M. Doring, V. Jamier and C. Jacob, *Org. Biomol. Chem.*, 2010, **8**, 4203–4216.
46 C. W. Nogueira, G. Zeni and J. B. T. Rocha, *Chem. Rev.*, 2004, **104**, 6255–6285.
47 W. Cao, Y. W. Gu, M. Meineck, T. Y. Li and H. P. Xu, *J. Am. Chem. Soc.*, 2014, **136**, 5132–5137.
48 W. Cao, L. Wang and H. P. Xu, *Nano Today*, 2015, **10**, 717–736.
49 L. Wang, W. Cao and H. P. Xu, *ChemNanoMat*, 2016, **2**, 479–488.
50 F. Li, T. Y. Li, C. X. Sun, J. H. Xia and H. P. Xu, *Biomaterials*, 2017, **133**, 208–218.
51 W. Cao, Y. W. Gu, T. Y. Li and H. P. Xu, *Chem. Commun.*, 2015, **51**, 7069–7071.

Published on 14 September 2018. Downloaded on 2/22/2026 8:50:49 PM.